High-Dimensional Manganese(II) Compounds with Noncovalent and/or Covalent Bonds Derived from Flexible Ligands: Self-Assembly and Structural Transformation

Chang Seop Hong,[†] Sang-Kil Son,[†] Yoon Sup Lee,[†] Moo-Jin Jun,[‡] and Youngkyu Do*[,†]

Department of Chemistry and Center for Molecular Science, Korea Advanced Institute of Science and Technology, Taejon 305-701, Korea, and Department of Chemistry, Yonsei University, Seoul 120-749, Korea

Received May 25, 1999

A hydrogen- and covalent-bonded 3D array, $[Mn(bpe)(H_2O)_4]_n(ClO_4)_{2n}(bpe)_{4n}(H_2O)_{2n}$ (**2**) [bpe = 1,2-bis(4-pyridyl)-ethane], a covalent-bonded 3D network, $[Mn(bpe)_{1.5}(H_2O)(tp)]_n(H_2O)_n$ (**3**) [tp = terephthalate], and a covalent-bonded 2D sheet, $[Mn(bpe)(N_3)_2]_n$ (**4**), have been synthesized and characterized by spectroscopic data and single-crystal X-ray diffraction studies. Complex **2** contains two types of packing bpe molecules: One type of bpe molecules (=N31-bpe and symmetry-related bpe) run along the chain direction, and the other type of bpe molecules (=N11-bpe and N21-bpe) are slanted to the chain linked by bridging bpe (=N1-bpe). The chain is coupled with hydrogen bonds via N31-bpe, while hydrogen bonds through packing bpe molecules of N11- and N21-bpe sew the chains, leading to a 3D interlocking network structure. The bpe ligands in **3** have an anti conformation for the bridging bpe and a gauche conformation for the capping bpe with a dihedral angle between the two pyridyl rings of 44.5°. The tp ligand acts as a linker of three metal ions through the unidentate and bridging modes, leading to the formation of a 2D layer. The final molecular dimensionality in **3** is determined from adding bpe ligands to the 2D sheet connected by tp ligands, resulting in a covalent-bonded 3D array where the bridging bpe ligands link the tp-bridged layers. The manganese(II) center in **4** consists of four equatorial azido nitrogen atoms and two axial bpe nitrogen atoms. The one-dimensional chains formed by two azido bridging ligands are interconnected by bpe ligands, each of which has two pyridyl rings with a dihedral angle of 67°, leading to a two-dimensional sheet. Variable-temperature magnetic susceptibility data of **2** and **4** have been fitted to the infinite-chain model ($H = -J\sum S_{Ai}\cdot S_{Ai+1}$) derived by Fisher under the molecular field approximation (J'). Obtained exchange parameters are $J = -0.083$ cm^{-1}, $g = 2.0$ for **2** and $J = -12.5$ cm^{-1}, $g = 2.0$, $J' = 1.3$ cm^{-1} for **4**. In the case of **3**, the magnetic nature was interpreted by the dimer model ($H = -JS_1\cdot S_2$), affording parameters $J = -0.96$ cm^{-1}, $g = 1.99$, $J' = -0.005$ cm^{-1}. MO calculations on a hypothetical dimeric unit $(NH_3)_5Mn-bpe-Mn(NH_3)_5$ are discussed to evaluate the magnetic nature for the bpe-bridged system **4**.

Introduction

Increasing attention has been paid to the construction of two-dimensional (2D) or three-dimensional (3D) magnetic systems in order to gain a better understanding of the correlation between structure and magnetism.[1] One strategy to build a spatially well-spanned framework, among others, is to utilize certain features of potentially bridging ligands, such as conformational flexibility, versatile binding modes, and the ability to form hydrogen bonds. In this regard, bpe (1,2-bis(4-pyridyl)ethane), tp (terephthalate), and azido ligands can be used as useful connectors to bridge paramagnetic centers into high-dimensional molecular arrangements.

The bpe ligand, which derives its structural versatility in the solid state from conformational flexibility and hydrogen bonding, has broad relevance to the construction of the solid-state architecture and crystal engineering.[2] The tp ligand can form multidimensional compounds owing to its multibinding ability with regard to metal ions.[3] Likewise, the azido ligand has two available coordination modes: end-on, known as a ferromagnetic interaction mode,[4] and end-to-end, known as an antiferromagnetic[4] or a ferromagnetic[5] coupling mode. In fact, our initial attempt at examining the synthetic strategy mentioned above was made by applying the proper combination of the flexible bpe with the tp ligand, leading to success in the preparation of a 3D manganese array, $[Mn(bpe)(H_2O)_4]_n(tp)_n(bpe)_{2n}$ (**1**), linked by the covalent and hydrogen bonds.[6]

Hydrogen bonding, which is the important directional interaction responsible for the supramolecular arrangement and the significant factor in crystal engineering,[7] has a drawback in the field of molecular magnetism since hydrogen-bonded systems

* Corresponding author. E-mail: ykdo@single.kaist.ac.kr.
† Korea Advanced Institute of Science and Technology.
‡ Yonsei University.

(1) (a) Stumf, H. O.; Ouahab, L.; Pei, Y.; Grandjean, D.; Kahn, O. *Science* **1993**, *261*, 447. (b) Miyasaka, H.; Matsumoto, N.; Okawa, H.; Re, N.; Gallo, E.; Floriani, C. *Angew. Chem., Int. Ed. Engl.* **1995**, *34*, 1446. (c) Kim, J.; Lim, J. M.; Choi, Y.-K.; Do, Y. *Angew. Chem., Int. Ed. Engl.* **1996**, *35*, 998.
(2) (a) Hennigar, T. L.; MacQuarrie, D. C.; Losier, P.; Rogers, R. D.; Zaworotko, M. J. *Angew. Chem., Int. Ed. Engl.* **1997**, *36*, 972. (b) Fujita, M.; Kwon, Y. J.; Miyazawa, M.; Oqura, K. *J. Chem. Soc., Chem. Commun.* **1994**, 1997. (c) Real, J. A.; Andres, E.; Munoz, M. C.; Julve, M.; Granier, T.; Bousseksou, A.; Varret, F. *Science* **1995**, *268*, 265.
(3) Hong, C. S.; Do, Y. *Inorg. Chem.* **1997**, *36*, 5684.
(4) (a) Escuer, A.; Vicente, R.; Ribas, J.; El Fallah, M. S.; Solans, X.; Font-Badía, M. *Inorg. Chem.* **1994**, *33*, 1842. (b) Vicente, R.; Escuer, A.; Ribas, J.; El Fallah, M. S.; Solans, X.; Font-Badía, M. *Inorg. Chem.* **1995**, *34*, 1278. (c) Ribas, J.; Monfort, M.; Ghosh, B. K.; Cortes, R.; Solans, X.; Font-Badía, M. *Inorg. Chem.* **1996**, *35*, 864.
(5) Hong, C. S.; Do, Y. *Angew. Chem., Int. Ed. Engl.* **1999**, *38*, 193.
(6) Hong, C. S.; Do, Y. *Inorg. Chem.* **1998**, *37*, 4470.

10.1021/ic990611w CCC: $18.00
Published on Web 11/10/1999

Scheme 1. Synthetic Routes to **1**−**4**.

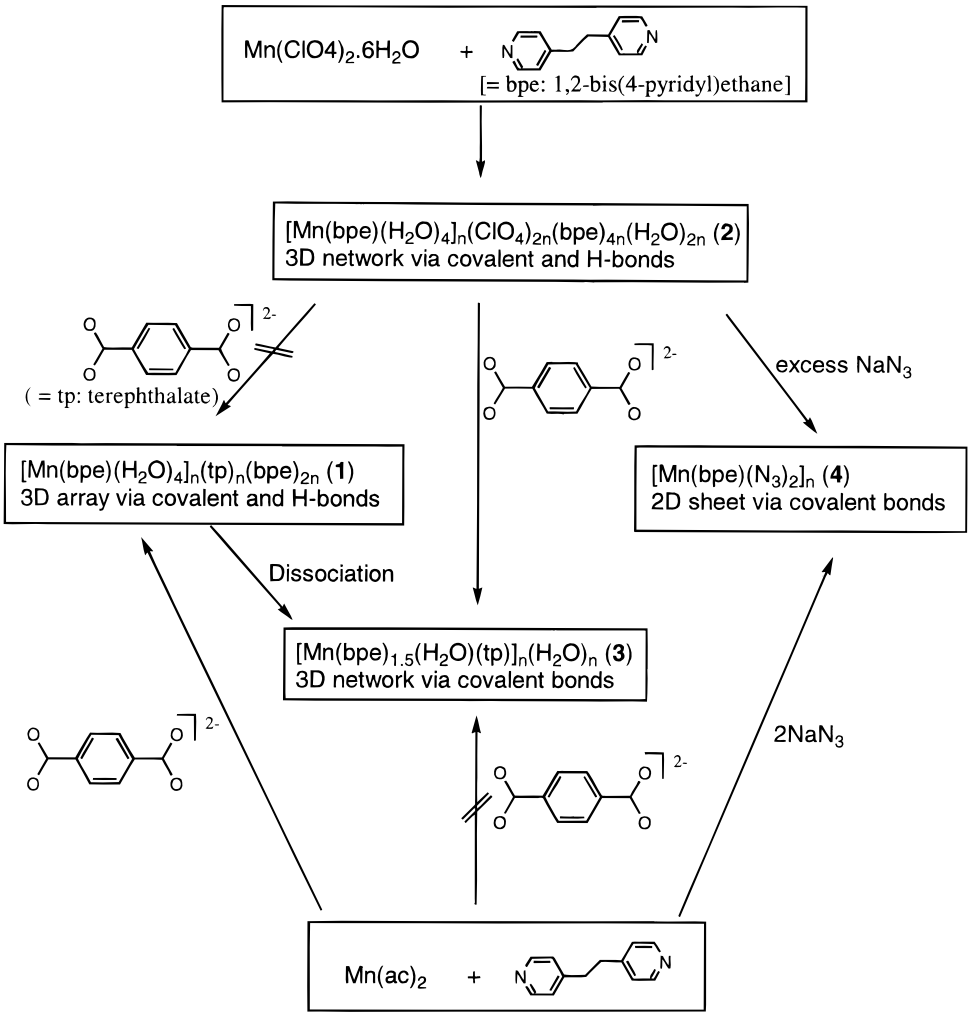

cannot provide enhanced magnetic interactions to the extent that covalent-bonded systems can. Therefore, the preparation of purely covalent-bonded high-dimensional systems is particularly crucial in the field of molecular magnets and the coupled use of two types of bridging ligands seems to be a reasonable synthetic strategy, but examples still remain scarce.[8] In addition, the transformation of noncovalent/covalent systems to high-dimensional covalent systems has not been well investigated. Thus, we explored these two aspects according to the synthetic routes outlined in Scheme 1 by employing the appropriate combinations of the ligands bpe, tp, and N_3^- and the hydrogen bond to attain new magnetically coupled systems with blended bridges. Herein, we report the syntheses, structures, and magnetic properties of a hydrogen- and covalent-bonded 3D array, $[Mn(bpe)(H_2O)_4]_n(ClO_4)_{2n}(bpe)_{4n}(H_2O)_{2n}$ (**2**), a covalent-bonded 3D network, $[Mn(bpe)_{1.5}(H_2O)(tp)]_n(H_2O)_n$ (**3**), and a covalent-bonded 2D sheet, $[Mn(bpe)(N_3)_2]_n$ (**4**) with two bridges. Molecular orbital (MO) model calculations for the bpe-bridged system were carried out to account for the magnetic mechanisms through the bpe bridge.

Experimental Section

Syntheses. $[Mn(bpe)(H_2O)_4]_n(ClO_4)_{2n}(bpe)_{4n}(H_2O)_{2n}$ (2). To an aqueous solution (10 mL) of manganese(II) perchlorate hexahydrate (0.50 mmol) was added a methanolic solution of bpe (0.50 mmol). The reaction mixture was stirred for 10 min at room temperature. The resulting mixture was filtered, and the filtrate was allowed to stand, giving, after several days, colorless crystals of **2** in 11% yield based on Mn. Anal. Calcd for $C_{60}H_{72}N_{10}O_{14}Cl_2Mn$: C, 56.17; H, 5.66; N, 10.92. Found: C, 56.34; H, 5.46; N, 11.15. Selected IR data (cm^{-1}, KBr pellet): 3613 (m), 3539 (m), 3055 (m, broad, several spikes present), 1944 (w), 1606 (s, bpe pyridyl skeletal), 1561 (m), 1502 (w), 1419 (m), 1223 (w), 1093 (vs, Cl−O stretching), 1005 (m), 827 (s), 812 (m), 663 (w), 622 (m), 547 (m), 529 (m), 497 (w).

$[Mn(bpe)_{1.5}(H_2O)(tp)]_n(H_2O)_n$ (3). To a solution of **2** (0.10 mmol) in 10 mL of methanol was added an aqueous solution of dipotassium tp (0.10 mmol). After 10 min of stirring, the reaction mixture was filtered, and the filtrate was left undisturbed. Well-formed colorless crystals of **3**, which were adequate for X-ray diffraction study, were obtained after several days in 94% yield based on Mn. Anal. Calcd for $C_{60}H_{70}N_{10}O_{13}Cl_2Mn$: C, 58.76; H, 4.93; N, 7.91. Found: C, 58.68; H, 4.93; N, 7.77. Selected IR data (cm^{-1}, KBr pellet): 3396 (m), 3235 (m, broad, several spikes present), 1986 (w), 1938 (w), 1653 (m), 1614 (vs, triplet, tp $\nu_a(CO_2^-)$), 1577 (vs, tp $\nu_a(CO_2^-)$), 1544 (s), 1500 (m), 1444 (m), 1427 (s), 1380 (vs, tp $\nu_s(CO_2^-)$), 1297 (m), 1227 (m), 1138 (w), 1092 (w), 1067 (w), 1017 (m), 929 (w), 897 (w), 866 (w), 830 (s), 758 (s), 650 (m), 599 (m), 546 (s), 514 (s). Compound **3** was also generated by allowing the hydrogen- and covalent-bond-linked 3D manganese array **1** in solid state to stand inside a desiccator equipped with $CaCl_2$ for several months at ambient temperature as confirmed by IR and elemental analysis.

$[Mn(bpe)(N_3)_2]_n$ (4). To an aqueous solution (10 mL) of manganese(II) acetate (0.50 mmol) was added a 10 mL methanolic solution of bpe (0.50 mmol). After being stirred for a few minutes, the reaction

(7) (a) Lehn, J.-M. *Angew. Chem., Int. Ed. Engl.* **1990**, *29*, 1304. (b) Palmans, A. R. A.; Vekemans, J. A. J. M.; Kooijman, H.; Speck, A. L.; Meijer, E. W. *Chem. Commun.* **1997**, 2247.
(8) De Munno, G.; Julve, M.; Viau, G.; Lloret, F.; Faus, J.; Viterbo, D. *Angew. Chem., Int. Ed. Engl.* **1996**, *35*, 1807.

Table 1. Crystallographic Data for **2**−**4**

	2	**3**	**4**
empirical formula	$C_{60}H_{72}N_{10}O_{14}Cl_2Mn$	$C_{26}H_{26}N_3O_6Mn$	$C_{12}H_{12}N_8Mn$
fw	1283.10	531.44	323.24
crystal system	triclinic	monoclinic	triclinic
space group	$P\bar{1}$	$P2_1/c$	$P\bar{1}$
a (Å)	14.045(1)	10.050(3)	8.558(2)
b (Å)	16.649(2)	11.963(4)	8.557(2)
c (Å)	17.028(2)	21.921(4)	10.501(1)
α (deg)	72.09(1)		97.65(1)
β (deg)	65.70(1)	92.72(4)	97.57(1)
γ (deg)	65.05(1)		108.53(1)
V (Å^3)	3246.8(7)	2632.7(13)	701.2(2)
Z	2	4	2
F(000)	1326	1104	330
d_{calcd} (g cm^{-3})	1.294	1.314	1.512
μ (mm^{-1})	0.353	0.545	0.936
scan mode	$\omega/2\theta$	$\omega/2\theta$	ω/θ
max 2θ (deg)	49.88	49.96	49.98
index range	$+h,\pm k,\pm l$	$+h,+k,\pm l$	$+h,\pm k,\pm l$
no. of tot. reflns	8782	2468	2071
no. of obsd reflections[a]	7422	1972	1569
no. of params	846	325	208
R1[b]	0.0628	0.0880	0.0593
wR2[c]	0.1723	0.1928	0.1338
weighting scheme:[c] x, y	0.1161, 1.9012	0.1219, 0	0.0600, 2.2275

[a] Criterion: $F_o > 4\sigma(F_o)$. [b] $R1 = \sum||F_o| - |F_c||/\sum|F_c|$. [c] $wR2 = \{\sum[w(F_o^2 - F_c^2)^2/\sum[w(F_o^2)^2]\}^{1/2}$, where $w = 1/[\sigma^2(F_o^2) + (xP)^2 + yP]$, $P = (F_o^2 + 2F_c^2)/3$.

mixture was treated with sodium azide (1.0 mmol) dissolved in 10 mL of water. Thirty minutes of stirring the resulting pale yellow solution was followed by filtration and standing of the filtrate. Pale yellow crystals of **4** suitable for X-ray diffraction were obtained in a yield of 56% based on Mn after several days of slow evaporation of the filtrate. Anal. Calcd for $C_{12}H_{12}N_8Mn$: C, 44.59; H, 3.74; N, 34.67. Found: C, 44.60; H, 3.74; N, 34.79. Selected IR data (cm^{-1}, KBr pellet): 3455 (w), 3380 (m), 3051 (w), 2937 (w), 2121 (vs, $\nu_a(N_3^-)$), 2069 (vs, $\nu_a(N_3^-)$), 1606 (s, bpe pyridyl skeletal), 1554 (m), 1500 (w), 1440 (w), 1426 (m), 1225 (m), 1069 (m), 1013 (m), 872 (w), 822 (m), 807 (m), 766 (w), 637 (m), 616 (w), 544 (m), 532 (m), 490 (m). Compound **4** was also obtained by treating **2** with excess sodium azide as confirmed by IR spectroscopy.

Physical Measurements. Elemental analyses for C, H, and N were performed at the Elemental Analysis Service Center of the Korea Basic Science Institute. Infrared spectra were obtained from KBr pellets with an EQUINOX 55 spectrometer. Thermal analyses (TGA) were performed under nitrogen atmosphere at a heating rate of 5 °C/min with DuPont TA instruments. Magnetic susceptibility measurements were carried out at the Korea Basic Science Institute using a Quantum Design MPMS-7 SQUID susceptometer. Corrections for the diamagnetism of the samples were estimated from Pascal's tables.[9]

Crystallographic Data Collection and Structure Determination. Data were collected at 293 K using an Enraf-Nonius CAD4TSB diffractometer with graphite-monochromated MoKα radiation (λ 0.710 73 Å) in the $\omega/2\theta$(**2**, **3**) or ω/θ (**4**) scan mode. The unit cell parameters were calculated by least-squares refinement of 25 for **2**, 23 for **3**, and 22 well-centered reflections for **4** in the ranges $21.34° < 2\theta < 26.72°$ (**2**), $19.85° < 2\theta < 31.45°$ (**3**), and $5.10° < 2\theta < 31.64°$ (**4**). All data were corrected for Lorentz−polarization effects. ψ-scan absorption corrections with transmission minimums and maximums of 94.44% and 99.97% for **3** and 98.67% and 99.94% for **4** were applied. Totals of 8782 (**2**), 2468 (**3**), and 2071 (**4**) reflections with the maximum 2θ values of 49.88° (**2**), 49.96 (**3**), and 49.98° (**4**) were measured, and 7422 (**2**), 1972 (**3**), and 1569 (**4**) reflections were assumed to be observed by applying the condition $F_o > 4\sigma(F_o)$. Crystallographic data and details of data collection are listed in Table 1.

The structures were solved with the SIR92 program[10] for **2** and the SHELXS-86 program[11] for **3** and **4** and refined by least-squares analysis using anisotropic thermal parameters for non-hydrogen atoms with the SHELXL-93 program for **2**−**4**.[12] The four oxygen atoms of the second perchlorate anion in **2** are disordered and were assigned a 0.25 occupancy factor. For **4**, two ethyl carbon atoms (C16 and C26) of the bpe ligand are disordered over two positions (C16′ and C26′) and were refined with a 0.5 occupancy factor. H atoms were calculated at idealized positions (d_{CH} = 0.970 Å for methylene and 0.930 Å for phenyl) and refined riding on the corresponding carbon atoms with isotropic thermal parameters [$U = 1.2U(C_{methylene})$ and $1.2U(C_{phenyl})$].

Results and Discussion

Synthesis and Characterization. The availability of compounds **2**−**4** depends on the type of the counteranion of manganese(II) salts employed. Outlined in Scheme 1 are the synthetic routes to these compounds as well as **1**, whose long-term stability in the solid state was not properly documented in our earlier report.[6]

The equimolar reaction of manganese(II) perchlorate hexahydrate with bpe led to **2** in a low yield of 11% based on Mn. Consideration of the Mn:bpe ratio in **2** suggests that bpe is likely the yield-limiting reagent and the yield is 55% based on bpe. The use of manganese(II) acetate instead of manganese(II) perchlorate hexahydrate did not give any tractable crystalline solids. In the IR spectrum of **2**, the sharp bands appearing at 3613 and 3539 cm^{-1} are attributed to unassociated O−H stretching bands of lattice water molecules while the hydrogen-bonded water molecules have the characteristic broad absorption around 3055 cm^{-1}. The strong peak centered at 1606 cm^{-1} is due to the presence of pyridyl skeletal vibrations of the bpe ligand.

The treatment of **2** with dipotassium tp or the serial treatment of manganese(II) perchlorate with bpe and then with dipotassium tp did not afford **1** but gave **3** in a high yield of 94%. On the other hand, when manganese(II) acetate was used instead of manganese(II) perchlorate, only the compound **1** was formed.[6] In addition, it should be noted that, in the solid state, compound **1** can be transformed into **3** by keeping **1** under dehydrating conditions at ambient temperature.

The IR spectrum of **3** shows two broad O−H stretching peaks at 3397 and 3234 cm^{-1}, indicating that all water molecules participate in hydrogen bonds over the lattice. The characteristic bands of the dicarboxylate units are shown in the usual region at 1614, 1578 cm^{-1} for antisymmetric stretching and at 1383 cm^{-1} for symmetric stretching. The differences between antisymmetric and symmetric stretchings correspond to 231 and 195 cm^{-1}, repectively, implying that the dicarboxylate units of the tp ligand function as unidentate as well as bridging units.[9] The TGA curve of **3** reveals that the loss of the lattice water molecules occurs in the range 73−108 °C with a weight loss of 3.5% (calculated value 3.4%); then the dehydration of coordinated water molecules follows in the temperature range 109−138 °C with a weight loss of 3.7%. The capping bpe ligand degrades at 145−200 °C with a loss of 16%, close to the theoretical value of 17%. The next decomposition process (36%) occurring in the temperature range 290−410 °C is assigned to the loss of the bridging bpe (calculated loss 35%), denoting that the bridging bpe is more stable than the capping bpe with respect to heating. The loss of the tp ligand occurs above 420 °C due to the strong bonds to metal ions. Heating to 800 °C

(9) Drago, R. S. *Physical Methods for Chemists*; Saunders College Publishing: New York, 1992; p 469.
(10) Altomare, A.; Cascarano, G.; Giacovazzo, C.; Guagliardi, A.; Burla, M. C.; Polidor, G.; Camallio, M. J. *J. Appl. Crystallogr.* **1994**, *27*, 435.
(11) Sheldrick, G. M. *SHELXS-86 User Guide*; Crystallographic Department, University of Göttingen: Göttingen, Germany, 1985.
(12) Sheldrick, G. M. *SHELXL-93 User Guide*; Crystallographic Department, University of Göttingen: Göttingen, Germany, 1993.

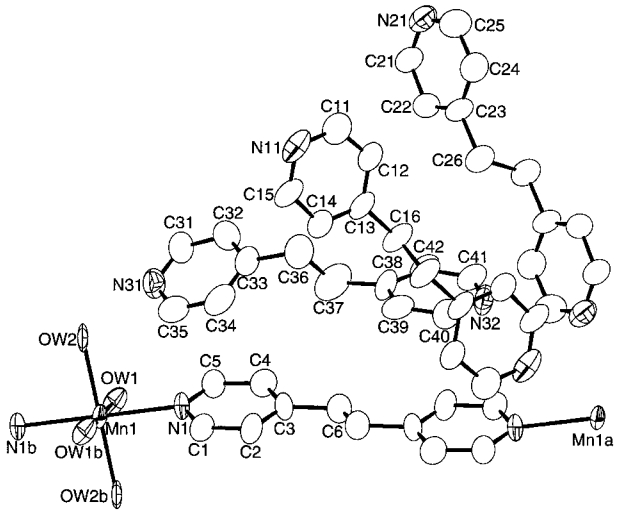

Figure 1. Molecular structure consisting of the repeating unit and part of the symmetry-related fragment of one of the two independent molecules of **2** in the asymmetric unit. The following symmetry codes are used to generate equivalent atoms: (a) $4 - x, 1 - y, -z$; (b) $3 - x, 1 - y, -z$.

Table 2. Selected Bond Distances (Å) and Angles (deg) for **2**

Mn1−OW1	2.150(2)	Mn1−OW2	2.188(2)
Mn1−N1	2.315(3)		
OW1−Mn1−OW2	89.42(10)	OW1−Mn1−N	189.96(10)
OW2−Mn1−N1	92.98(12)	C1−N1−Mn1	121.4(3)
C5−N1−Mn1	123.4(3)		

gave a brown solid which is likely to be manganese oxide in view of the IR spectrum.

The preparation of **4** was accomplished by two pathways. The first synthetic route is the same as that of **1** except for the use of 2 equiv of sodium azide instead of dipotassium tp. It is also possible to prepare **4** by reacting **2** with excess sodium azide. In this case, the stoichiometric reaction proved unsuccessful. The IR spectrum of **4** as a KBr pellet shows two very strong absorptions at 2121 and 2069 cm^{-1} attributable to the $\nu_a(N_3^-)$ stretching vibration of coordinated azide, indicating the presence of a twisted configuration and/or an end-to-end binding mode for the azide.[13,14]

Description of the Structures. $[Mn(bpe)(H_2O)_4]_n(ClO_4)_{2n}\cdot(bpe)_{4n}(H_2O)_{2n}$ (2). Figure 1 represents the molecular structure consisting of the repeating unit and part of the symmetry-related fragment of one of the two independent molecules of **2** in the asymmetric unit. The perchlorate counteranions, the packing water molecule, and the symmetry-related molecule of the fully labeled packing bpe molecule are omitted in Figure 1 for clarity. Selected bond distances and angles are reported in Table 2.

The Mn center lies in a distorted octahedral arrangement in which the axial positions are occupied by nitrogen atoms (N1 and N1b) of the bridging bpe ligands with Mn−N1 = 2.315(3) Å and the equatorial ones are defined by four water molecules (OW1, OW2, OW1b, and OW2b) with Mn1−OW1 = 2.150(2) and Mn1−OW2 = 2.188(2) Å. Each axial N1-bpe ligand bridges Mn(II) ions, forming an 1D chain with an intrachain intermanganese distance of 14.045 Å. Among four packing bpe molecules, two bpe molecules (N31-bpe and its symmetry-related bpe) run along the chain direction while the other two (N11-bpe and N21-bpe) slant against the chain. It is interesting to note that the conformational flexibility of bpe seen in **1** is also observed in **2**.[6] All the bpe ligands in **2** show an anti conformation. The bridging bpe ligand possesses parallel pyridyl rings with an interplanar distance of ca. 0.62 Å whereas the slanted coplanar packing bpe molecules adopt longer interplanar distances of ca. 1.30 Å for N11-bpe and ca. 1.38 Å for N21-bpe. In the case of N31-bpe running parallel with the chain, the pyridyl rings are tilted toward each other to form a dihedral angle of 29.8°.

Shown in Figure 2a, omitting the slanted bpe molecules of N11- and N21-bpe for clarity, shows the chain bridged by the N1-bpe ligand with an Mn···Mn distance of 14.045 Å. The metal centers are additionally interconnected with hydrogen bonds between the coordinated water molecules and the parallel bpe molecules (OW2···N31 = 2.814 and OW2···N32e = 2.846 Å; e = $-1 + x, y, z$). Figure 2b is a partially extended view where the slanted bpe molecules are included and the orientation is taken such that the chains illustrated in Figure 2a run into the paper. The slanted bpe molecules interconnect manganese centers belonging to the different chains via hydrogen bonds with the coordinated water molecules (OW1···N11c = 2.777 and OW1···N21d = 2.749 Å; c = $3 - x, 1 - y, 1 - z$ and d = $x, -1 + y, z$), giving rise to the 3D network structure with an interlocking feature as depicted in Figure 2c and Chart 1. In Figure 2c, the perchlorate counteranions and packing water molecules, which are located near hexagon-like channels formed by stacking of the slanted bpe molecules and the coordinated water molecules, are discrete from the remaining 3D network and thus are omitted for clarity. The shortest interchain Mn··· Mn distance is 9.910 Å.

$[Mn(bpe)_{1.5}(H_2O)(tp)]_n(H_2O)_n$ (3). An ORTEP representation of **3** at the 50% probability level is shown in Figure 3. Selected bond distances and angles are reported in Table 3.

The Mn ion has a distorted octahedral geometry consisting of two nitrogen atoms from trans bpe ligands with bond distances of Mn1−N11 = 2.288(5) and Mn1−N31 = 2.266(5) Å and three oxygen atoms from tp ligands and one oxygen atom from the water molecule with bond distances of Mn1−O1 = 2.151(4), Mn1−O2a = 2.146(5), Mn1−O3c = 2.198(4), and Mn1−OW1 = 2.218(5) Å. The bpe ligands in **3** are also conformationally flexible and adopt an anti conformation for the bridging N11-bpe with an interplanar distance of ca. 1.48 Å and a gauche conformation for the capping N31-bpe with a dihedral angle of 44.5° between the two pyridyl rings. In particular, the gauche conformation of the capping bpe is stabilized by the hydrogen bond between N41 and the lattice water (OW2···N41e = 2.952 Å; e = $1 - x, 0.5 + y, 0.5 - z$). The tp ligand acts as a linker of three metal ions through the unidentate and bridging modes, which is consistent with the interpretation of the IR spectrum. The inter-manganese distances via extended tp and bpe ligands are 4.848 Å for Mn1···Mn1a, 11.086 Å for Mn1···Mn1b, 10.998 Å for Mn1a···Mn1b, 13.811 Å for Mn1···Mn1d, and 15.642 Å for Mn1a···Mn1d.

The overall 3D network feature of **3** can be illustrated in following stepwise manner. Removal of the bpe molecules in **3** leads to the stacked sheet system, and Figure 4a shows one of such 2D sheets running in the *bc* plane. It is evident that manganese centers in the sheet are coordinatively linked by tp bridges and the additional hydrogen-bonding interactions occur among nonligating oxygen atoms of the tp ligand, the coordinated water molecule, and the lattice water (O4···OW1b = 2.724, OW1···OW2f = 2.780, and O4···OW2g = 2.845 Å; f

(13) Nakamoto, K. *Infrared and Raman Spectra of Inorganic and Coordination Compounds. Part B: Application in Coordination, Orgnometallic, and Bioinorganic Chemistry*, 5th ed.; Wiley: New York, 1997.

(14) Cortes, R.; Drillon, M.; Solans, X.; Lezama, L.; Rojo, T. *Inorg. Chem.* **1997**, *36*, 677.

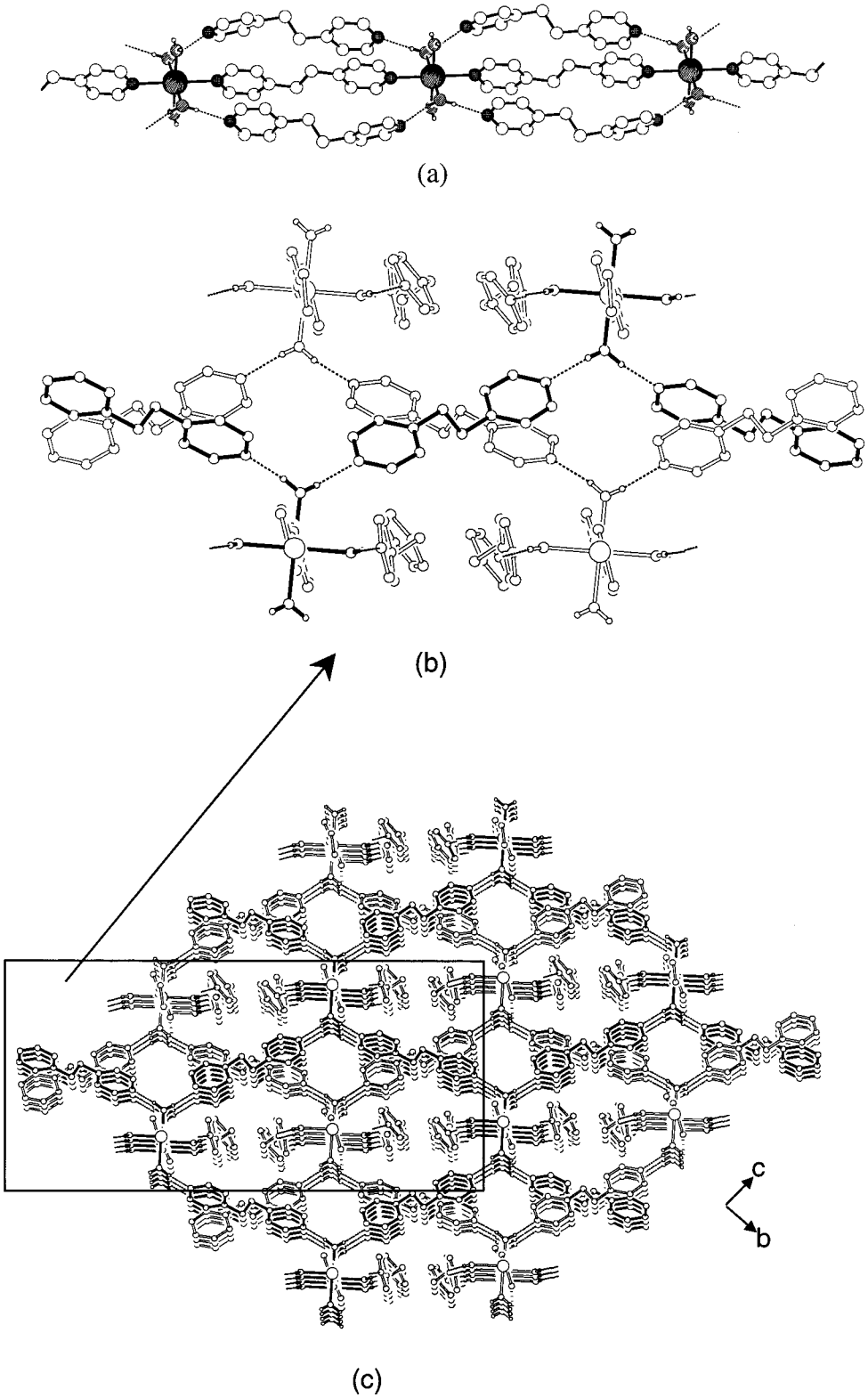

Figure 2. (a) View of the manganese 1D chain for **2**. (b) Partially extended molecular view of **2**, showing the interlocking feature. (c) Overall 3D molecular view of **2**.

$= 1 - x, 1 - y, -z$ and g $= x, 0.5 - y, -0.5 + z$), forming hexagons in the open space of the 2D sheet. The inclusion of the bpe molecules which connect sheets affords the final molecular dimensionality of **3** as shown in Figure 4b.

$[Mn(bpe)(N_3)_2]_n$ (4). The molecular structure of **4**, which is consistent with the spectroscopic observations, is depicted in Figure 5. Selected bond distances and angles are reported in Table 4.

The manganese(II) ion has a distorted octahedral environment, formed by four equatorial azido nitrogen atoms and two axial bpe nitrogen atoms. The average Mn−N(azido) bond distance of 2.223 Å is shorter than that of Mn−N(bpe) (2.264 Å). The Mn−azido angles of Mn−N−N, very important structural parameters from the magnetic point of view, are 136.9 and 137.1°. The Mn ions are connected by two azido bridging ligands, forming one-dimensional chains with an inter-manga-

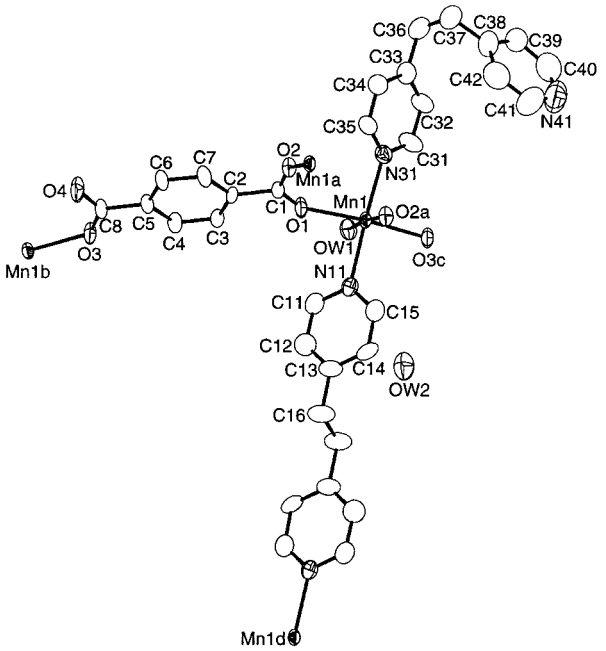

Figure 3. ORTEP drawing of **3** with the atom-numbering scheme. The following symmetry codes are used to generate equivalent atoms: (a) $1 - x, -y, -z$; (b) $x, 0.5 - y, 0.5 - z$; (c) $x, 0.5 - y, 0.5 + z$; (d) $2 - x, 1 - y, -z$.

Chart 1. Representation of an Interlocking Feature in **2**

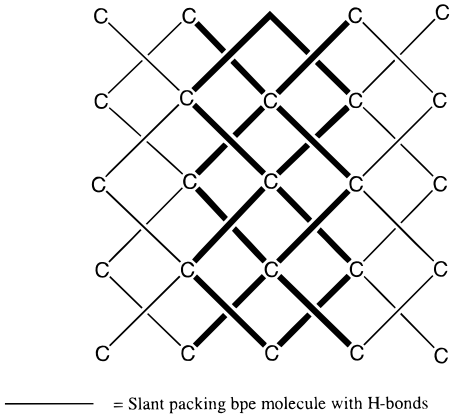

= Slant packing bpe molecule with H-bonds

C = Manganese(II) chains shown in Figure 2a

Table 3. Selected Bond Distances (Å) and Angles (deg) for **3**

Mn1−O2	2.146(5)	Mn1−O	12.151(4)
Mn1−O3	2.198(4)	Mn1−O5	2.218(5)
Mn1−N31	2.266(5)	Mn1−N11	2.288(5)
O2−Mn1−O1	99.1(2)	O2−Mn1−O3	91.7(2)
O1−Mn1−O3	168.6(2)	O2−Mn1−O5	174.0(2)
O1−Mn1−O5	85.3(2)	O3−Mn1−O5	83.6(2)
O2−Mn1−N31	90.7(2)	O1−Mn1−N31	95.4(2)
O3−Mn1−N31	87.9(2)	O5−Mn1−N31	93.0(2)
O2−Mn1−N11	86.5(2)	O1−Mn1−N11	86.5(2)
O3−Mn1−N11	90.6(2)	O5−Mn1−N11	89.7(2)
N31−Mn1−N11	176.8(3)	C1−O1−Mn1	139.5(4)
C1−O2−Mn1	146.7(4)	C8−O3−Mn1	130.6(4)
C15−N11−Mn1	121.7(4)	C11−N11−Mn1	121.2(6)
C35−N31−Mn1	120.2(3)	C31−N31−Mn1	123.6(5)

nese distance of 5.337 Å along the chains. These chains are interconnected by bpe ligands, each of which has two pyridyl rings with a dihedral angle of 67°, affording a two-dimensional sheet. The interdistance between Mn ions connected through the bpe ligand is 13.893 Å, slightly shorter than that (13.993 Å) found in the hydrogen- and covalent-bonded 3D complex **1** where the two pyridyl rings of the bpe ligand are coplanar.[6] The resulting sheets are stacked along the *a* axis to give the layered crystal structure of **4** as shown in Figure 6. This clearly shows that two types of bridging ligands play an important role in constructing a higher dimensional system, which is synthetically interesting from the molecular architectural and magnetic point of view.

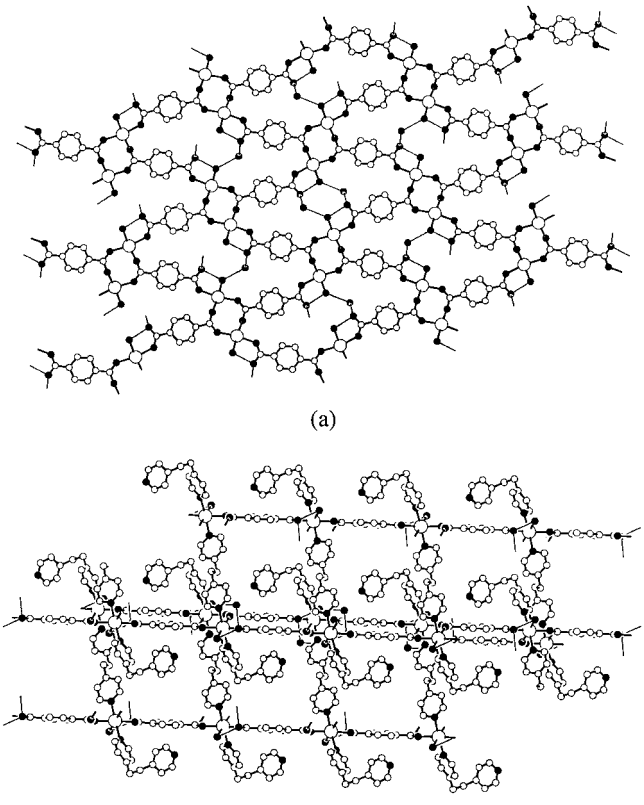

Figure 4. Views of (a) the 2D sheet running in the *bc* plane and (b) the 3D network of **3**.

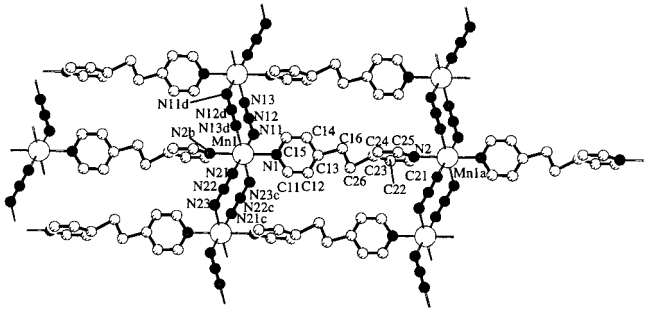

Figure 5. Perspective view of **4** with the atomic numbering scheme. Symmetry codes used to generate equivalent atoms: (a) $-1 + x, 1 + y, z$; (b) $1 + x, -1 + y, z$; (c) $1 - x, -y, -z$; (d) $1 - x, -y, 1 - z$.

Table 4. Selected Bond Distances (Å) and Angles (deg) for **4**

Mn1−N1	2.252(6)	Mn1−N11	2.218(6)
Mn1−N21	2.204(6)	Mn1−N2b	2.276(6)
Mn1−N23c	2.234(6)	Mn1−N13d	2.236(6)
N11−Mn1−N(21	179.7(2)	N11−Mn1−N23c	89.5(2)
N11−Mn1−N13d	90.4(2)	N21−Mn1−N23c	90.8(2)
N13d−Mn1−N21	89.3(2)	N13d−Mn1−N23c	178.4(2)
Mn1−N11−N12	136.9(5)	Mn1−N21−N22	137.1(5)

Magnetism. $[Mn(bpe)(H_2O)_4]_n(ClO_4)_{2n}(bpe)_{4n}(H_2O)_n$ (2). The magnetic susceptibility for **2** was measured in the range

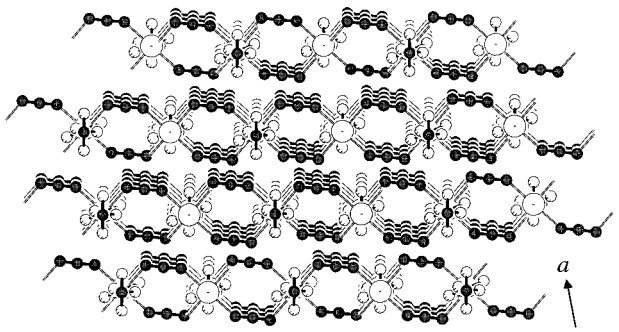

Figure 6. Layered structure of **4** stacked along the *a* axis.

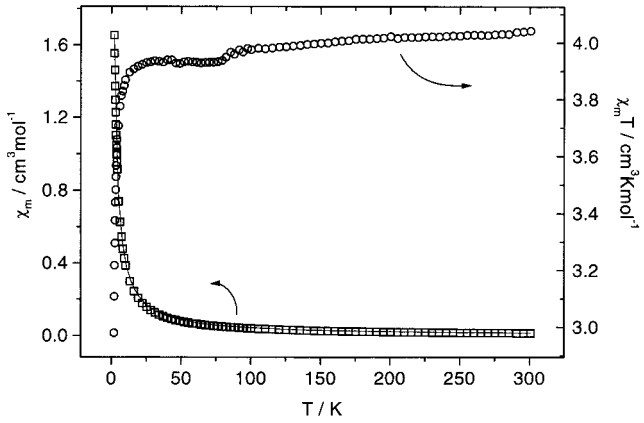

Figure 7. Plots of χ_m and χ_mT versus T for **2**. The solid line represents the best theoretical fit.

1.8−300 K, as seen in Figure 7. At room temperature, compound **2** has a χ_mT value of 4.04 cm^3 K mol^{-1}, lower than that of the noninteracting Mn(II) entities. The χ_mT value decreases slowly and then abruptly below 16 K to reach a value of 2.98 cm^3 K mol^{-1}, typical of antiferromagnetic behavior.

The interpretation of the variation of the experimental magnetic data with temperature was attempted by using the infinite-chain model ($H = -J\sum S_{Ai}\cdot S_{Ai+1}$) derived by Fisher[15] as expressed in eq 1, with $u = \coth[JS_A(S_A + 1)/kT] - [kT/JS_A(S_A + 1)]$.

$$\chi_m = [Ng^2\beta^2S_A(S_A + 1)/3kT][(1 + u)/(1 - u)] \qquad (1)$$

The parameters obtained from the fit of the experimental values with eq 1 using $S_A = {}^5/_2$ are $J = -0.083$ cm^{-1} and $g = 2.0$. The measure of the goodness of fit R, defined as $R = [\Phi/(n - k)]^{1/2}$ where n is the number of data points, k is the number of parameters, and $\Phi = \sum[(\chi_m)_i^{obs} - (\chi_m)_i^{calc}]^2$ is equal to 8.4×10^{-3}. The weakness of the exchange coupling can be explained by the large distance between the magnetic centers in a chain. It appears that the smaller J value of **2** compared with that ($J = -0.84$ cm^{-1}) of **1** is due to the larger intrachain distance (13.993 Å for **1** and 14.045 Å for **2**) between magnetic centers and/or the larger interplanar distance (ca. 0.5 Å for **1** and ca. 0.62 Å for **2**) between two pyridyl rings in the bridging bpe ligand.[6]

$[Mn(bpe)_{1.5}(H_2O)(tp)]_n(H_2O)_n$ (3). The temperature dependence of the magnetic susceptibility per $[Mn(bpe)_{1.5}(H_2O)(tp)]_2(H_2O)_2$ unit of **3** in the form of χ_m vs T together with χ_mT vs T is shown in Figure 8. The χ_m value keeps increasing as temperature decreases, reaches a maximum value of 0.615 cm^3 mol^{-1} at 4.8 K, and then decreases down to a value of 0.582 cm^3 mol^{-1} at 2 K. The χ_mT value per 2Mn at 300 K is 8.80 cm^3 K mol^{-1}, which is in accord with the spin-only value in the absence of any exchange interaction. Upon cooling, the χ_mT value decreases very slowly down to a value of 8.54 cm^3 K mol^{-1} at 100 K and then decreases rapidly from 7.74 cm^3 K mol^{-1} at 35 K to 1.06 cm^3 K mol^{-1} at 1.8 K. This is characteristic of an overall antiferromagnetic phenomenon.

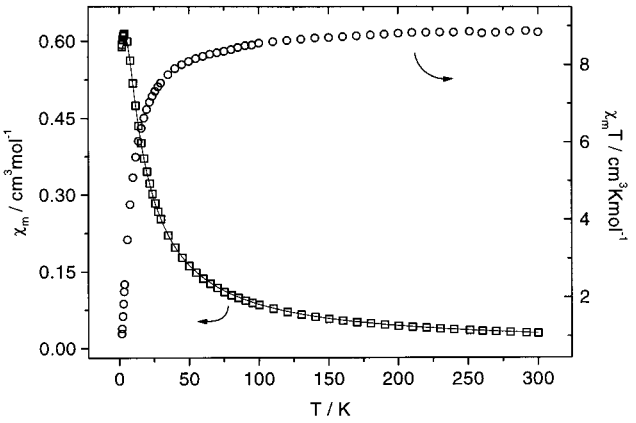

Figure 8. Plots of χ_m and χ_mT versus T for **3**. The solid line represents the best theoretical fit.

There are three possible magnetic pathways based on the crystal structure of **3**: the first through carboxylate moieties of tp units, the second via the benzene backbones of tp ligands, and the last through the bpe bridge. The major contribution to the magnetic behavior observed in **3** would be made by the first magnetic route owing to the shortest distance between magnetic centers. In this criterion, we simplified the magnetic system to the exchange coupling in a dinuclear Mn(II) unit bridged by the carboxylate groups of tp ligands. The solution to the Van Vleck expression using the isotropic Heisenberg Hamiltonian for the dimanganese(II) entity written as $H = -JS_1\cdot S_2$ ($S_1 = S_2 = {}^5/_2$) yields the magnetic susceptibility χ_m described in eq 2,[16]

$$\chi_m = [2Ng^2\beta^2/kT][(e^x + 5e^{3x} + 14e^{6x} + 30e^{10x} + 55e^{15x})/(1 + 3e^x + 5e^{3x} + 7e^{6x} + 9e^{10x} + 11e^{15x})] \qquad (2)$$

where $x = J/kT$.

Because of the extended network via the second and third pathways, the molecular field approximation was added, and the final expression of the magnetic susceptibility is given by eq 3. The magnetic parameters obtained from the fitting

$$\chi_m(MF) = \chi_m/[1 - (2zJ'/Ng^2\beta^2)\chi_m] \qquad (3)$$

procedure are $J = -0.96$ cm^{-1}, $g = 1.99$, and $J' = -0.005$ cm^{-1} with $R = 1.9 \times 10^{-3}$. On the basis of this model, the antiferromagnetic interactions are present in **3** as expected for the carboxylate bridged systems. The exchange coupling parameter (J) is similar to that of doubly bridged carboxylate manganese(II) complexes.[3,17] The small interdimer parameter (J') is attributable to the contribution through the benzene rings of tp ligands and bpe bridges.

$[Mn(bpe)(N_3)_2]_n$ (4). The thermal dependence of the molar magnetic susceptibility (χ_m) in the temperature range 5−300 K is shown in Figure 9. When the sample is cooled, χ_m rapidly

(15) Fisher, M. E. *Am. J. Phys.* **1964**, *32*, 343.

(16) Hong, C. S.; Kim, J.; Hur, N. H.; Do, Y. *Inorg. Chem.* **1996**, *35*, 5510.

(17) Cano, J.; De Munno, G.; Sanz, J. L.; Ruiz, R.; Faus, J.; Lloret, F.; Julve, M.; Caneschi, A. *J. Chem. Soc., Dalton Trans.* **1997**, 1915.

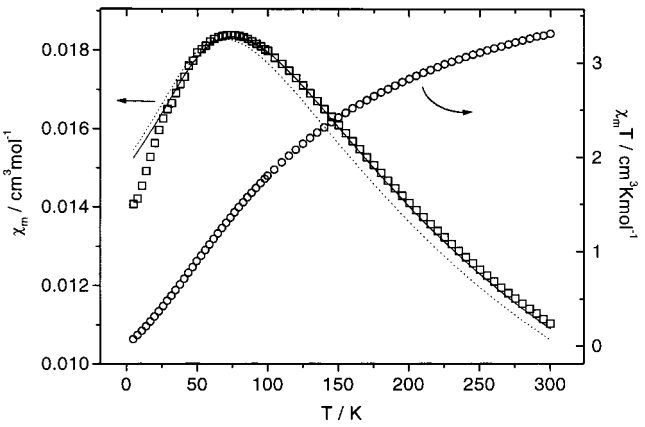

Figure 9. Plots of χ_m and $\chi_m T$ versus T for **4**. The solid and dotted lines represent the best theoretical fits.

increases, reaches a round maximum near 74 K, and then abruptly decreases, indicating the existence of an overall antiferromagnetic interaction in a two-dimensional sheet. The $\chi_m T$ value at 300 K is equal to 3.31 cm^3 K mol^{-1}, which is already lower than the calculated value of 4.38 cm^3 K mol^{-1} for the noncoupled Mn(II) ion. When the temperature is lowered further, the $\chi_m T$ value continuously decreases and finally reaches a value of 0.0703 cm^3 K mol^{-1} at 5 K, typical of antiferromagnetic behavior.

There are two possible magnetic exchange pathways on the sheet in **4**: one is through the azido ligand and the other is via the bpe ligand. Considering that the dominant factor which governs the magnetic character of **4** would be a short-distance mediator between the magnetic centers, the overall antiferromagnetism in **4** should result from the azido bridge rather than from the bpe ligand. Placing the focus for the interpretation of magnetic properties of **4** on the azido ligand, we attempted an analysis of the magnetic susceptibility data by using eq 1. The best fit of the magnetic data leads to the parameters $g = 2.08$ and $J = -12.5$ cm^{-1}. Although R is acceptable as 3.2×10^{-4}, the g factor obtained above is rather too large.

When the g value for the Mn(II) ion with $S_A = {}^5/_2$ is fixed as 2.0, the exchange parameter is estimated to be $J = -11.5$ cm^{-1} and $R = 4.9 \times 10^{-4}$. Shown in Figure 9 as a dotted line is the least-squares fitting curve which is lower than the data points in the high-temperature region ($T > 74$ K), indicating the presence of a ferromagnetic contribution in this system. As a matter of fact, the possible involvement of the bpe bridge ligand in magnetic exchange in **4** cannot be simply ruled out since the presence of a weak magnetic interaction via the coordinatively bridging bpe ligand was seen in $[Mn(bpe)(H_2O)_4]_n(tp)_n(bpe)_{2n}$ (**1**), where two adjacent paramagnetic centers are 13.993 Å separated by the bpe ligand.[6] The inclusion of the interchain interaction (J') via the bpe bridge under the consideration of the molecular field approximation (eq 3) into eq 1 leads to the parameters $g = 2.0$, $J = -12.5$ cm^{-1}, $J' = 1.3$ cm^{-1}, and $R = 2.9 \times 10^{-4}$. The solid line in Figure 9 demonstrates a better agreement of the theoretical results with the experimental data. The negative sign for J is as expected since the end-to-end type azido bridge can mediate magnetic couplings whose natures are dependent mainly on the angle between Mn and the azido ligand and the average Mn−N−N bond angle of 137° for **4** substantially deviates from 165°, which is the estimated value for the accidental orthogonality.[18] The magnitude of the J value of **4** falls into the usual range observed for end-to-end azido-dibridged Mn(II) compounds.[14] The positive J' value denotes that the bpe ligand may mediate the weak ferromagnetic coupling. The deviation of the theoretical consequence from the experimental data points in the low-temperature region implies the presence of an antiferromagnetic contribution between 2D sheets of **4**.

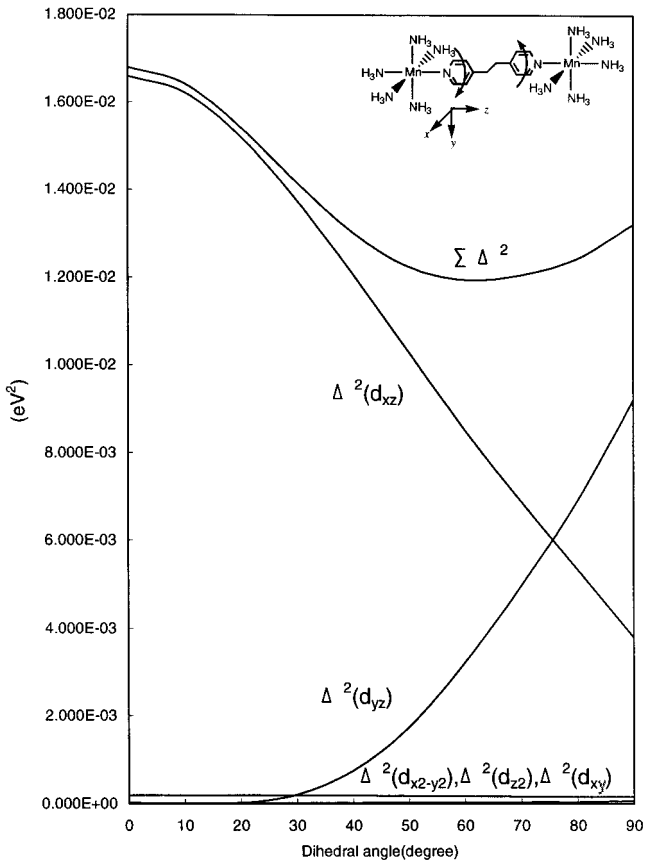

Figure 10. Plot of the variation of the square gap (Δ^2) versus the dihedral angle between the two pyridyl rings of the bpe ligand. The inset shows a scheme of the hypothetical dimeric model.

MO Calculations. To clarify the magnetic nature of the bpe ligand in **4**, the correlation between the bridging bpe conformation and magnetic properties of bpe-mediated magnetic systems was explored by performing MO calculations at the EHT level on the hypothetical dimeric unit $(NH_3)_5Mn-bpe-Mn(NH_3)_5$ taken as a close mimic of $N_5Mn-bpe-MnN_5$ unit in **4**. Since the antiferromagnetic component is a function of the sum of the squares of the energy gaps between the magnetic orbitals on a d^5-d^5 system,[18] that is $\sum\Delta^2 = \Delta^2(d_{z^2}) + \Delta^2(d_{x^2-y^2}) + \Delta^2(d_{xy}) + \Delta^2(d_{xz}) + \Delta^2(d_{yz})$ where $\Delta^2 = |\Phi_a - \Phi_s|^2$, the dependence of $\sum\Delta^2$ on the variation of the dihedral angle between the two pyridyl rings of the bpe ligand was calculated. The d_{z^2} orbital is oriented parallel to the Mn−N(bpe) direction and the d_{yz} orbital is placed in the same plane with the two pyridyl rings before the rotation. Two pyridyl groups are rotated simultaneously in opposite directions with the $Mn(NH_3)_5$ moieties fixed. As illustrated in Figure 10, the change in the energy gaps mainly arises from the d_{xz} and d_{yz} orbitals and the minimum of $\sum\Delta^2$ is observed in the dihedral angle range 60−70°. This minimum signifies the minimal antiferromagnetic contribution (J_{ij}AF) in a simple exchange between pairs of magnetic orbitals [$J = (1/n^2)\Sigma_{ij}J_{ij}$; $J_{ij} = J_{ij}^F(>0) + J_{ij}^{AF}(<0)$],[19]

(18) (a) Escuer, A.; Vicente, R.; Goher, M. A. A.; Mautner, F. A. *Inorg. Chem.* **1996**, *35*, 6386. (b) Escuer, A.; Vicente, R.; Goher, M. A. A.; Mautner, F. A. *Inorg. Chem.* **1998**, *37*, 782.

(19) Kahn, O. *Molecular Magnetism*; VCH: New York, 1993; p 185.

implying that the superexchange through the bpe ligand is more likely to become ferromagnetic near the dihedral angles between 60 and 70° than other angles. In fact, it is interesting to note that the pyridyl rings of the bpe bridge in **1**−**3** are parallel, which allows antiferromagntic interactions, while in the case of **4** the bridging bpe has tilted pyridyl planes with a dihedral angle of 67°, which makes antiferromagnetic contribution minimal and thus ferromagnetic contribution dominant. Hence, the foregoing simple MO treatment seems to be in favor of supporting the role of the long-pathway bpe as a weak ferromagnetic coupling mediator in **4**. However, the lack of a reported example with ferromagnetic bpe bridging mediators hampers making any further conclusion on the magnetic behavior of the bpe ligand in **4**. Attempts at synthesizing high-dimensional systems in which paramagnetic centers are coordinatively connected only by bpe ligands with dihedral angles of 60−70° between pyridyl planes are in progress.

Conclusions

In this paper, we have demonstrated the synthetic significance of the coupled use of two types of bridging ligands in preparing purely covalent-bonded high-dimensional systems and the transformation of noncovalent/covalent systems to high-dimensional covalent systems as manifested by the preparation of three new multidimensional compounds of a hydrogen- and covalent-bonded 3D array, $[Mn(bpe)(H_2O)_4]_n(ClO_4)_{2n}(bpe)_{4n}(H_2O)_{2n}$ (**2**), a covalent-bonded 3D network, $[Mn(bpe)_{1.5}(H_2O)(tp)]_n(H_2O)_n$ (**3**), and a covalent-bonded 2D sheet, $[Mn(bpe)(N_3)_2]_n$ (**4**). Complex **2** is a useful precursor since additional bridges can be incorporated into the framework of **2** to construct compounds **3** and **4** with blended bridging ligands and intriguing magnetic properties. In view of the solid structure, complex **3** is more stable than a 3D manganese array, $[Mn(bpe)(H_2O)_4]_n(tp)_n(bpe)_{2n}$ (**1**), under dehydrating conditions at ambient temperature, as evidenced by the structural transformation of complex **1** into **3**. It is interesting to note that three roles of the bpe ligand in the molecular structures of **1**−**4** are observed as bridging, capping, and packing. This conformational flexibility would allow the higher dimensional entities found in the present work.

Magnetic studies of **2**−**4** show magnetic exchange coupling parameters of $J = -0.083$ cm^{-1} through the bpe bridge for **2** and $J = -0.96$ cm^{-1} via doubly bridged carboxylate motifs and an interdimer exchange constant $J' = -0.005$ cm^{-1} for **3**. In the case of **4**, there are two magnetic pathways with different magnetic natures: $J = -12.5$ cm^{-1} through end-to-end azido ligands and $J' = 1.3$ cm^{-1} mediated by the bpe ligand with the tilted pyridyl rings. The fascinating role of bpe as a ferromagnetic mediator in **4** was evaluated by performing MO calculations at the EHT level on the hypothetical dimeric unit $(NH_3)_5Mn-bpe-Mn(NH_3)$.

Acknowledgment. The authors acknowledge financial support from the Korea Research Foundation in the program year of 1997.

Supporting Information Available: Tables giving atomic coordinates, isotropic thermal parameters, anisotropic thermal parameters, and bond distances and angles for **2**−**4**. This material is available free of charge via the Internet at http://pubs.acs.org.

IC990611W